# Higher-Order Topology and Nodal Topological Superconductivity in Fe(Se,Te) Heterostructures

Rui-Xing Zhang,[1,*] William S. Cole,[1] Xianxin Wu,[2] and S. Das Sarma[1]
[1]Condensed Matter Theory Center and Joint Quantum Institute, Department of Physics, University of Maryland, College Park, Maryland 20742-4111, USA
[2]Institut für Theoretische Physik und Astrophysik, Universität Würzburg, Am Hubland Campus Süd, Würzburg 97074, Germany

(Received 12 June 2019; revised manuscript received 28 August 2019; published 17 October 2019)

We show, theoretically, that a heterostructure of monolayer $FeTe_{1-x}Se_x$—a superconducting quantum spin Hall material—with a monolayer of FeTe—a bicollinear antiferromagnet—realizes a higher order topological superconductor phase characterized by emergent Majorana zero modes pinned to the sample corners. We provide a minimal effective model for this system, analyze the origin of higher order topology, and fully characterize the topological phase diagram. Despite the conventional $s$-wave pairing, we find a rather surprising emergence of a novel topological nodal superconductor in the phase diagram. Featured by edge-dependent Majorana flat bands, the topological nodal phase is protected by an antiferromagnetic chiral symmetry. We also discuss the experimental feasibility, the estimation of realistic model parameters, and the robustness of the Majorana corner modes against magnetic and potential disorder. Our work provides a new experimentally feasible high-temperature platform for both higher order topology and non-Abelian Majorana physics.

DOI: 10.1103/PhysRevLett.123.167001

*Introduction.*—For the past decade, iron-based superconductors have been a central research theme in condensed matter physics, owing to their high superconducting (SC) transition temperature $T_c$, rich phase diagrams, and in particular, the puzzle of the origin of pairing [1–7]. While the underlying microscopic mechanisms of SC in both bulk and monolayer iron-based superconductors remain controversial, remarkable progress has been made recently towards revealing their nontrivial topological properties [8–16]. As the prototypical example of a topological iron-based superconductor, bulk $FeTe_{1-x}Se_x$ (FTS) with $x = 0.45$ hosts a helical Dirac surface state above $T_c$, as confirmed by angle-resolved photoemission spectroscopy (ARPES) measurements [12,14]. Below $T_c$, strong evidence for Majorana vortex bound states has been found reproducibly in several scanning tunneling microscopy (STM) experiments [13,16–18], following from the theoretical prediction of surface topological superconductivity developed via a "self-proximity" effect [19]. Similar to its bulk counterpart, the normal-state band structure of monolayer FTS has been theoretically predicted to be topological [10]. This prediction is further supported by a recent systematic ARPES measurement of monolayer FTS [20,21], clearly revealing a bulk topological phase transition (band gap closing at Γ) by continuously changing the value of $x$. With the highest $T_c$ among iron-based superconductors [22–24], one might wonder whether FTS monolayer also offers a new high temperature platform for topological Majorana physics. It should be noted, however, that the coexistence of nontrivial band topology and SC does not guarantee topological superconductivity (TSC). In fact, two-dimensional (2D), time-reversal invariant TSC requires very strict conditions for both the Fermi surface geometry and SC pairing symmetry [25,26]. With the puzzle of pairing symmetry unresolved [27], the question of TSC in monolayer FTS remains open, although the answer is very likely negative.

In this Letter, we provide an alternative pairing-symmetry-independent route to obtain Majorana bound states in monolayer FTS systems. We demonstrate that Majorana zero modes emerge at physical corners of a sample when a FeTe layer is deposited on top of the FTS monolayer, as shown in Fig. 1(b). The bicollinear antiferromagnetic (AFM) order of FeTe [28–31] is the key enabling higher order topology [32–53] in this heterostructure binding

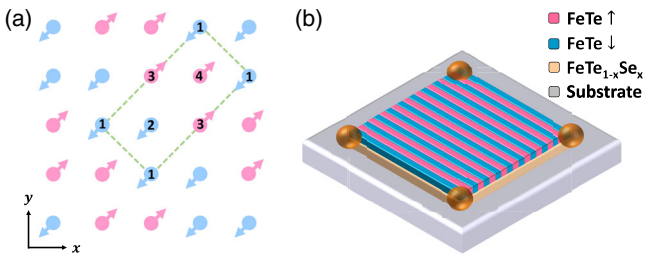


FIG. 1. (a) Schematic plot of bicollinear antiferromagnetic order in FeTe. The circle and its arrow represent the Fe atom and its magnetic moment. (b) Schematic plot of the FTS/FeTe heterostructure with corner-localized Majorana modes.

 

localized Majorana zero modes, without relying on the choice of pairing symmetry. This heterostructure-based mechanism is essentially different from our earlier proposal for bulk FTS, where the higher order topology is enabled by unconventional $s_\pm$ pairing [54]. We construct a minimal lattice model to explain the origin of higher order topology in this heterostructure, and we also study the stability of Majorana corner modes with respect to finite chemical potential $\mu$ and disorder effects. In the large $\mu$ limit, the FeTe layer also enables a novel topological nodal SC phase with symmetry protected edge Majorana flat bands, even when the SC pairing is singlet $s$ wave.

*Model Hamiltonian.*—The low-energy theory of monolayer FTS around the $\Gamma$ point is a superconducting version of the Bernevig-Hughes-Zhang (BHZ) model [10,55]. While the pairing mechanism in monolayer iron chalcogenide systems is still under debate, a conventional $s$-wave singlet pairing $\Delta$ will suffice for our purpose. The Hamiltonian for FTS is then

$$h_{\mathrm{BHZ}} = [(m-4B)+2B(\cos\, k_x+\cos\, k_y)]\Gamma_5 - \mu\Gamma_{67} + A(\sin\, k_x\Gamma_{167} - \sin\, k_y\Gamma_2) + \Delta\Gamma_{137}, \quad (1)$$

in terms of a choice of $8\times 8$ $\Gamma$ matrices

$$\begin{aligned} &\Gamma_1 = \tau_z\otimes\sigma_x\otimes s_z, && \Gamma_2 = \tau_z\otimes\sigma_y\otimes s_0,\\ &\Gamma_3 = \tau_z\otimes\sigma_x\otimes s_x, && \Gamma_4 = \tau_z\otimes\sigma_x\otimes s_y,\\ &\Gamma_5 = \tau_z\otimes\sigma_z\otimes s_0, && \Gamma_6 = \tau_x\otimes\sigma_0\otimes s_0,\\ &\Gamma_7 = \tau_y\otimes\sigma_0\otimes s_0, \end{aligned} \quad (2)$$

with $\Gamma_{jk}=\Gamma_j\Gamma_k/i$ and $\Gamma_{jkl}=\Gamma_j\Gamma_k\Gamma_l/i$ for $j\neq k\neq l\in\{1,2,\ldots,8\}$. Here, $s$, $\sigma$, and $\tau$ Pauli matrices denote spin, orbital, and particle-hole degrees of freedom, respectively. $m$, $B$, and $A$ are hopping parameters that follow the convention of the BHZ model. When $0<m<8B$, the normal-state part of $h_{\mathrm{BHZ}}$ is topologically nontrivial and possesses helical edge modes. However, the $s$-wave SC pairing necessarily trivializes the band topology of the full Bogoliubov-de Gennes (BdG) model.

Covering the FTS monolayer with a monolayer FeTe introduces an exchange coupling with the bicollinear AFM order of FeTe to the system. Unlike a conventional collinear AFM, the magnetic moments in the bicollinear AFM flip their orientation every two atoms along the diagonal direction (e.g., the [11] direction) [28], as shown in Fig. 1(a). As a result, the unit cell is enlarged to contain four inequivalent atoms, labeled by a sublattice index $i=1,2,3,4$. The new unit cell is characterized by the lattice vectors $\tilde{\mathbf{a}}_x=2(\mathbf{a}_x+\mathbf{a}_y)$, $\tilde{\mathbf{a}}_y=-\mathbf{a}_x+\mathbf{a}_y$, where $\mathbf{a}_{x,y}$ are the lattice vectors of the original square lattice BHZ model. $k_{\tilde{x}}$ and $k_{\tilde{y}}$ denote the crystal momenta in the folded Brillouin zone, and we will use $M$ to represent the interlayer exchange coupling between FTS and FeTe. The matrix form of the full Hamiltonian $H_{\mathrm{FTS}}$ with both SC and AFM is shown in the Supplemental Material [56].

*Majorana corner modes.*—To understand the emergence of topological Majorana zero modes in our system, it is instructive to switch off superconductivity first and study the topological consequence of the bicollinear AFM. Despite explicitly breaking the time-reversal symmetry $\Theta$, introducing AFM to a quantum spin Hall system does not necessarily destroy the helical edge states. Instead, these edge states are now protected by an effective time-reversal symmetry $\Theta_M=\Theta e^{ik_{\tilde{x}}/2}$, which combines $\Theta$ with a half-unit-cell translation along $\mathbf{a}_{\tilde{x}}$. As shown in Fig. 1(a), $\Theta_M$ swaps electrons of index $i=1,2$ with those of $i=3,4$. Therefore, $\Theta_M$ is a magnetic space group operation and has a crucial difference from the conventional time-reversal symmetry $\Theta$ [57–59]: the Kramers degeneracy of $\Theta_M$ only arises at the high symmetry points with $k_{\tilde{x}}=0$.

Because of the crystalline nature of $\Theta_M$, not every edge preserves $\Theta_M$ and is capable of hosting helical edge states. In particular, as shown in Fig. 1(a), the magnetic configuration of the $\tilde{\mathbf{y}}$ edge (which is parallel to $\tilde{\mathbf{a}}_y$) is ferromagnetic (FM), which locally breaks $\Theta_M$ and produces an edge magnetic gap. This is in contrast to gapless edges (such as the $\tilde{\mathbf{x}}$ edge) with AFM ordering and $\Theta_M$ protection. To verify this picture, we have used the iterative Green function method to numerically calculate the edge dispersion with finite exchange coupling $M$ and zero $\Delta$ for both $\tilde{\mathbf{x}}$ and $\tilde{\mathbf{y}}$ edges. As shown in Fig. 2(a), the $\tilde{\mathbf{x}}$ edge has a Kramers degeneracy at $\tilde{\Gamma}$ (with $\Theta_M^2=-1$) but not at $\tilde{X}$ (with $\Theta_M^2=+1$). Meanwhile, Fig. 2(b) clearly shows the magnetic gap at $\tilde{\Gamma}$ on the $\tilde{\mathbf{y}}$ edge, which follows our expectation.

Now, we include SC in our discussion. Through the self-proximity effect accompanying the development of bulk SC in the FTS layer, the gapless $\tilde{\mathbf{x}}$ edge opens a SC gap. For the $\tilde{\mathbf{y}}$ edge, however, there exists a competition between the edge FM gap and the edge SC gap. In particular, when the FM gap dominates the $\tilde{\mathbf{x}}$ edge, the corner between $\tilde{\mathbf{x}}$ and $\tilde{\mathbf{y}}$ edges represents a zero-dimensional domain wall between SC and FM gaps, which necessarily binds a single Majorana zero mode to the corner [60,61], thus, enabling higher order topology.

Therefore, the higher order topology in the heterostructure is controlled by the character of the $\tilde{\mathbf{y}}$ edge gap where SC and FM compete. This motivates us to construct an effective theory of the $\tilde{\mathbf{y}}$ edge that describes the competition between FM and SC,

$$h_{\tilde{\mathbf{y}}} = k_{\tilde{y}}\tau_0\otimes\sigma_z + \delta_M\tau_z\otimes\sigma_x + \Delta\tau_y\otimes\sigma_y - \mu\tau_z\otimes\sigma_0. \quad (3)$$

Here, $\delta_M$ is the effective exchange coupling on the $\tilde{\mathbf{y}}$ edge, which originates from the edge projection of the bulk AFM order $M$. While it is generally difficult to analytically express $\delta_M$ in terms of $M$, we numerically confirm a simple linear relation with $\delta_M\approx\beta_M M$. The linear coefficient $\beta_M$ depends on the details of hopping parameters, and we find

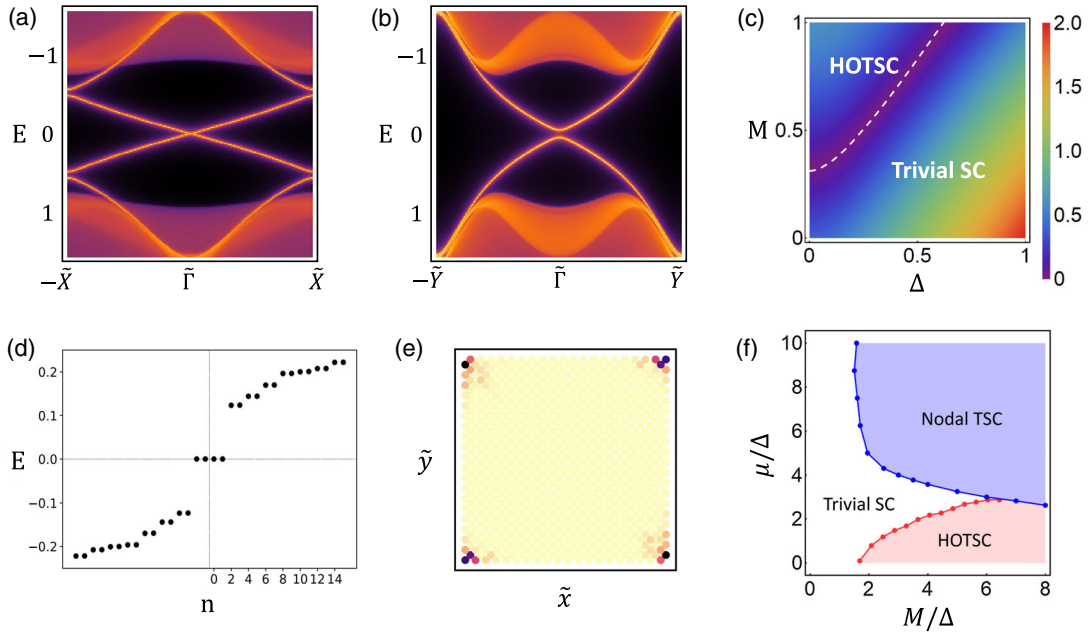


FIG. 2. With $(A, B, m, M, \Delta) = (1, 1, 2, 0.2, 0)$, dispersions of $\tilde{x}$ edge (AFM) and $\tilde{y}$ edge (FM) are plotted in (a) and (b), respectively. (c) Topological phase diagram for a fixed $\mu = 0.2$. The white dashed line shows the analytical results of Eq. (4). (d) Energy spectrum of $H_{\mathrm{FTS}}$ with open boundary conditions in both $\tilde{x}$ and $\tilde{y}$ directions, which clearly reveals four Majorana zero modes. (e) Spatial profile of the Majorana zero modes in (d). (f) Topological phase diagram with respect to $M$ and $\mu$ at a fixed $\Delta$.

$\beta_M \simeq 0.678$ for our choice of parameters. For nonzero $\delta_M$ and $\Delta$, the edge topological phase transition occurs when the energy gap of $h_{\tilde{\mathbf{y}}}$ closes. Thus, the topological condition of a higher order topological superconductor (HOTSC) is given by [56],

$$M^2 > \frac{1}{\beta_M^2}(\mu^2 + \Delta^2), \tag{4}$$

when FM exceeds SC on the $\tilde{\mathbf{y}}$ edge. To further confirm Eq. (4), we numerically map out the energy gap distribution in the parameter space spanned by $M$ and $\Delta$ at a fixed $\mu$. As shown in Fig. 2(c), the topological phase transition predicted by Eq. (4) (white dashed line) agrees well with the color map of the edge gap from a numerical nanoribbon calculation (where the gap closing regions are labeled in purple).

Following this topological criterion, we calculate the eigenvalues of $H_{\mathrm{FTS}}$ on a $20\tilde{a}_y \times 10\tilde{a}_x$ open cluster by direct diagonalization. As shown in Fig. 2(d), in the topological phase at $(M, \Delta, \mu) = (0.6, 0.2, 0.0)$, four Majorana zero modes are found to live inside the edge gap. We plot the combined spatial profile of these four zero modes in Fig. 2(e), and additionally confirm that they are exponentially localized at the corners of the system. These corner localized 0D Majorana bound states are the hallmark of higher order topology in this 2D system.

*Emergent nodal TSC.*—In the small $\mu$ limit, the edge topological condition in Eq. (4) provides a simple analytical diagnostic for the appearance of Majorana corner modes. To explore the fate of higher order topology at finite $\mu$, we fix the value of $\Delta$ and numerically map out the topological phase diagram tuning $M$ and $\mu$. In Fig. 2(f), the HOTSC phase and the trivial phase are denoted by the red and white regions, respectively. The phase boundary that separates the HOTSC and trivial SC corresponds to the gap closing of FM edge. In addition, an emergent nodal superconducting phase (blue region) is found to dominate the phase diagram when both $\mu$ and $M$ are large. Since only conventional $s$-wave singlet pairing is considered in our model, this nodal structure is unusual and emerges from the combined effects of AFM and SC.

The origin of the emergent nodal SC can be understood by projecting $s$-wave pairing onto the bulk Fermi surface. At zero $M$, the effective pairing gap $\Delta_{\mathrm{FS}}(\mathbf{k})$ is always uniform on the Fermi surface (FS), which simply signals the uniform, isotropic $s$-wave pairing. As $M$ is turned on from zero, the Fermi surface develops a spin texture such that $\Delta_{\mathrm{FS}}(\mathbf{k})$ becomes anisotropic in the Brillouin zone and, thus, develops momentum contours with $\Delta_{\mathrm{FS}}(\mathbf{k}) = 0$. For example, the Fermi surface for $(M, \Delta, \mu) = (0.6, 0.2, 1.2)$ is mapped out in Fig. 3(a), which clearly shows the position of SC nodes in the spectrum. As a comparison, we plot the Fermi surface of the normal band structure alone in Fig. 3(b), along with the calculated zero-pairing contours (white dashed lines). As expected, the BDG spectrum has nodal points where the zero-pairing contour intersects the normal state Fermi surface.

These emergent bulk SC nodes carry a nontrivial topological charge and, thus, lead to interesting boundary

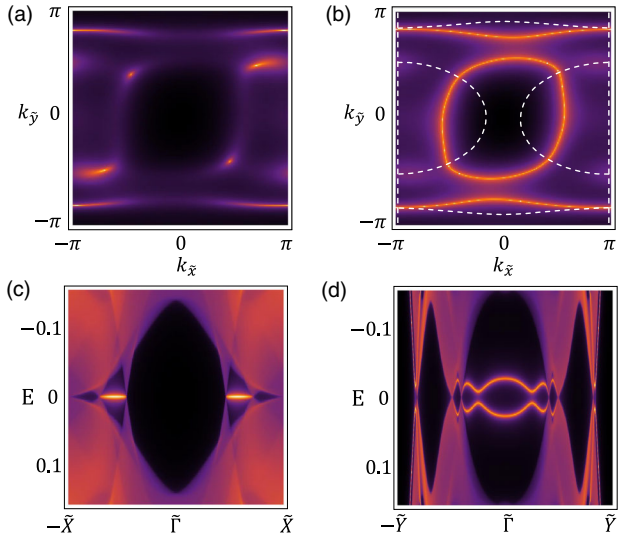


FIG. 3. (a) Position of SC nodes in the Brillouin zone for the nodal SC phase. (b) Fermi surface of the corresponding normal band structure and the zero-pairing contours (white dashed lines). (c) and (d) show the dispersions of the AFM edge and the FM edge for the nodal SC phase, respectively. The AFM edge hosts symmetry protected Majorana flat bands.

Majorana physics. By combining the effective time-reversal symmetry $\Theta_M$ and particle-hole symmetry $\Pi$, an AFM chiral symmetry operation is defined as

$$\mathcal{C} = \Theta_M \Pi, \tag{5}$$

which anticommutes with $H_{\mathrm{FTS}}$. The AFM chiral symmetry allows us, in turn, to define a topological charge $Q$ [56,62,63], and we find numerically

$$|Q| = 2, \tag{6}$$

for every SC node.

The bulk-boundary correspondence then implies the existence of edge Majorana flat bands between SC nodes with opposite topological charges in a nanoribbon geometry. In Figs. 3(c) and 3(d), we show the calculated edge spectrum for the AFM $\tilde{x}$ edge and FM $\tilde{y}$ edge, respectively. As expected, the $\tilde{x}$ edge hosts zero-energy Majorana flat bands between the projections of the nodal points. These Majorana flat bands are doubly degenerate due to $|Q| = 2$. Crucially, the AFM chiral symmetry prevents any coupling between the degenerate flat bands, which further protects their Majorana nature [56]. On the $\tilde{y}$ edge, however, the AFM chiral symmetry is explicitly broken because of the absence of $\Theta_M$. Therefore, the internode edge modes are not protected by $\mathcal{C}$ and, therefore, need not be pinned to zero energy. As expected, the edge modes in Fig. 3(d) are found to hybridize with each other with a nonzero splitting which shifts the modes from zero energy. The edge-dependent Majorana flat bands are a unique feature of the AFM chiral symmetry-protected nodal TSC phase.

*Feasibility of experimental realization.*—Now, we discuss the experimental feasibility of our proposal. First, we notice that the fabrication techniques for iron chalcogenide heterostructures are well-developed [23,64,65]. In particular, bilayers of different iron chalcogenide layers (for example, a FeSe layer and a FeTe layer) were found to be coherently constrained to each other [65], which should hold in our proposed $\mathrm{FeTe}_{1-x}\mathrm{Se}_x$/FeTe bilayer as well. The precise epitaxial lattice matching between different iron chalcogenide layers greatly facilitates the edge characterization and identification of a corner Majorana signal in realistic materials.

We also attempt to make some realistic estimates on the energy scales of physical quantities involved in the topological condition of Eq. (4). ARPES studies on the monolayer FeSe system reveal a SC gap $\Delta$ of about 10 meV [66]. The magnetic structure of FeTe has been measured in Refs. [29,30], which leads to local magnetic moments about 1.65 $\mu_B$ along the $b$ axis (parallel spin axis), where $\mu_B$ is the Bohr magneton. The local magnetic moment of the FeTe layer induces a magnetic proximity effect through exchange coupling with the FTS layer. To evaluate the scale of the induced exchange coupling, we perform a first-principles calculation of a bilayer FeSe system, introducing ferromagnetism to the top FeSe layer [56]. With a magnetic moment of 2.76 $\mu_B$, the proximity-induced exchange coupling of the bottom layer is around 100 meV. Thus, for the experimentally observed magnetic moment of 1.65 $\mu_B$ in FeTe, the induced exchange coupling in the FTS layer is expected to be $M \approx 60$ meV. Given that $\beta_M \sim 0.5$, the edge FM potential is still much greater than the edge SC potential, and thus, the topological condition for Majorana corner modes is always satisfied for a small chemical potential.

*Conclusion and discussion.*—We have established the higher order TSC phase with Majorana corner modes in monolayer Fe(Se,Te) heterostructures, together with an emergent symmetry-protected nodal TSC phase. In addition to our proposed heterostructure being feasible to create, both the Majorana corner modes and the dispersing Majorana edge flat bands exhibit distinct features in local spectroscopy and, therefore, should be experimentally visible using standard STM techniques. Our proposed realization of Majorana corner modes does not rely on fine-tuning of the chemical potential, nor does it require perfect ordering of moments in the FeTe layer. In the Supplemental Material [56], we consider a disordered model with a fixed density of magnetic defects where $\pm M \to \mp M$, which explicitly breaks $\Theta_M$, and we find that the corner modes persist even for a substantial defect density. Finally, unlike most previous proposals for HOTSC [42–44,54], our setup does not require an unconventional pairing symmetry. Rather, the combination of

AFM and conventional *s*-wave pairing effectively mimics anisotropic pairing leading to generic HOTSC. However, it would be interesting (and possibly experimentally relevant for FTS) to generalize to unconventional pairing. In fact, the full landscape of trivial vs topological normal state band structure, uniform vs nonuniform magnetism, and conventional vs unconventional pairing symmetry appears to be quite rich and already at hand in iron-based materials.

R.-X. Z is indebted to Chao-Xing Liu, Jiabin Yu, Fengcheng Wu, and Biao Lian for helpful discussions. This work is supported by the Laboratory for Physical Sciences and Microsoft. R.-X. Z. is supported by a JQI Postdoctoral Fellowship.

*Note added.*—We have recently become aware of a related work on the monolayer FTS, where the higher order topology is driven by an in-plane magnetic field [67].

*ruixing@umd.edu

[1] Y. Kamihara, T. Watanabe, M. Hirano, and H. Hosono, J. Am. Chem. Soc. **130**, 3296 (2008).
[2] T. Hanaguri, S. Niitaka, K. Kuroki, and H. Takagi, Science **328**, 474 (2010).
[3] J. Paglione and R. L. Greene, Nat. Phys. **6**, 645 (2010).
[4] F. Wang and D.-H. Lee, Science **332**, 200 (2011).
[5] P. J. Hirschfeld, M. M. Korshunov, and I. I. Mazin, Rep. Prog. Phys. **74**, 124508 (2011).
[6] A. Chubukov, Annu. Rev. Condens. Matter Phys. **3**, 57 (2012).
[7] A. Chubukov and P. J. Hirschfeld, Phys. Today **68**, No. 6, 46 (2015).
[8] N. Hao and J. Hu, Phys. Rev. X **4**, 031053 (2014).
[9] X. Wu, S. Qin, Y. Liang, C. Le, H. Fan, and J. Hu, Phys. Rev. B **91**, 081111(R) (2015).
[10] X. Wu, S. Qin, Y. Liang, H. Fan, and J. Hu, Phys. Rev. B **93**, 115129 (2016).
[11] G. Xu, B. Lian, P. Tang, X.-L. Qi, and S.-C. Zhang, Phys. Rev. Lett. **117**, 047001 (2016).
[12] P. Zhang, K. Yaji, T. Hashimoto, Y. Ota, T. Kondo, K. Okazaki, Z. Wang, J. Wen, G. D. Gu, H. Ding, and S. Shin, Science **360**, 182 (2018).
[13] D. Wang, L. Kong, P. Fan, H. Chen, S. Zhu, W. Liu, L. Cao, Y. Sun, S. Du, J. Schneeloch, R. Zhong, G. Gu, L. Fu, H. Ding, and H.-J. Gao, Science **362**, 333 (2018).
[14] P. Zhang *et al.*, Nat. Phys. **15**, 41 (2019).
[15] N. Hao and J. Hu, Natl. Sci. Rev. **6**, 213 (2019).
[16] T. Machida, Y. Sun, S. Pyon, S. Takeda, Y. Kohsaka, T. Hanaguri, T. Sasagawa, and T. Tamegai, Nat. Mater. **18**, 811 (2019).
[17] L. Kong, S. Zhu, M. Papaj, L. Cao, H. Isobe, W. Liu, D. Wang, P. Fan, H. Chen, Y. Sun *et al.*, arXiv:1901.02293.
[18] S. Zhu, L. Kong, L. Cao, H. Chen, S. Du, Y. Xing, W. Liu, D. Wang, C. Shen, F. Yang *et al.*, arXiv:1904.06124.
[19] L. Fu and C. L. Kane, Phys. Rev. Lett. **100**, 096407 (2008).
[20] X. Shi, Z.-Q. Han, P. Richard, X.-X. Wu, X.-L. Peng, T. Qian, S.-C. Wang, J.-P. Hu, Y.-J. Sun, and H. Ding, Sci. Bull. **62**, 503 (2017).
[21] X.-L. Peng, Y. Li, X.-X. Wu, H.-B. Deng, X. Shi, W.-H. Fan, M. Li, Y.-B. Huang, T. Qian, P. Richard *et al.*, arXiv:1903.05968.
[22] W. Qing-Yan, L. Zhi, Z. Wen-Hao, Z. Zuo-Cheng, Z. Jin-Song, L. Wei, D. Hao, O. Yun-Bo, D. Peng, C. Kai *et al.*, Chin. Phys. Lett. **29**, 037402 (2012).
[23] Z. Wen-Hao, S. Yi, Z. Jin-Song, L. Fang-Sen, G. Ming-Hua, Z. Yan-Fei, Z. Hui-Min, P. Jun-Ping, X. Ying, W. Hui-Chao *et al.*, Chin. Phys. Lett. **31**, 017401 (2014).
[24] J.-F. Ge, Z.-L. Liu, C. Liu, C.-L. Gao, D. Qian, Q.-K. Xue, Y. Liu, and J.-F. Jia, Nat. Mater. **14**, 285 (2015).
[25] X.-L. Qi, T. L. Hughes, S. Raghu, and S.-C. Zhang, Phys. Rev. Lett. **102**, 187001 (2009).
[26] F. Zhang, C. L. Kane, and E. J. Mele, Phys. Rev. Lett. **111**, 056402 (2013).
[27] D. Huang and J. E. Hoffman, Annu. Rev. Condens. Matter Phys. **8**, 311 (2017).
[28] F. Ma, W. Ji, J. Hu, Z.-Y. Lu, and T. Xiang, Phys. Rev. Lett. **102**, 177003 (2009).
[29] W. Bao, Y. Qiu, Q. Huang, M. Green, P. Zajdel, M. Fitzsimmons, M. Zhernenkov, S. Chang, M. Fang, B. Qian *et al.*, Phys. Rev. Lett. **102**, 247001 (2009).
[30] S. Li, C. de La Cruz, Q. Huang, Y. Chen, J. W. Lynn, J. Hu, Y.-L. Huang, F.-C. Hsu, K.-W. Yeh, M.-K. Wu *et al.*, Phys. Rev. B **79**, 054503 (2009).
[31] S. Manna, A. Kamlapure, L. Cornils, T. Hänke, E. Hedegaard, M. Bremholm, B. Iversen, P. Hofmann, J. Wiebe, and R. Wiesendanger, Nat. Commun. **8**, 14074 (2017).
[32] W. A. Benalcazar, B. A. Bernevig, and T. L. Hughes, Science **357**, 61 (2017).
[33] W. A. Benalcazar, B. A. Bernevig, and T. L. Hughes, Phys. Rev. B **96**, 245115 (2017).
[34] F. Zhang, C. L. Kane, and E. J. Mele, Phys. Rev. Lett. **110**, 046404 (2013).
[35] F. Schindler, A. M. Cook, M. G. Vergniory, Z. Wang, S. S. Parkin, B. A. Bernevig, and T. Neupert, Sci. Adv. **4**, eaat0346 (2018).
[36] J. Langbehn, Y. Peng, L. Trifunovic, F. von Oppen, and P. W. Brouwer, Phys. Rev. Lett. **119**, 246401 (2017).
[37] E. Khalaf, Phys. Rev. B **97**, 205136 (2018).
[38] T. Liu, J. J. He, and F. Nori, Phys. Rev. B **98**, 245413 (2018).
[39] Y. Peng and Y. Xu, Phys. Rev. B **99**, 195431 (2019).
[40] H. Shapourian, Y. Wang, and S. Ryu, Phys. Rev. B **97**, 094508 (2018).
[41] Y. Volpez, D. Loss, and J. Klinovaja, Phys. Rev. Lett. **122**, 126402 (2019).
[42] Q. Wang, C.-C. Liu, Y.-M. Lu, and F. Zhang, Phys. Rev. Lett. **121**, 186801 (2018).
[43] Z. Yan, F. Song, and Z. Wang, Phys. Rev. Lett. **121**, 096803 (2018).
[44] Y. Wang, M. Lin, and T. L. Hughes, Phys. Rev. B **98**, 165144 (2018).
[45] Z. Wu, Z. Yan, and W. Huang, Phys. Rev. B **99**, 020508(R) (2019).
[46] X. Zhu, Phys. Rev. B **97**, 205134 (2018).
[47] N. Bultinck, B. A. Bernevig, and M. P. Zaletel, Phys. Rev. B **99**, 125149 (2019).
[48] X.-H. Pan, K.-J. Yang, L. Chen, G. Xu, C.-X. Liu, and X. Liu, arXiv:1812.10989 [Phys. Rev. Lett. (to be published)].

[49] S. A. A. Ghorashi, X. Hu, T. L. Hughes, and E. Rossi, Phys. Rev. B **100**, 020509 (2019).
[50] S. Franca, D. Efremov, and I. Fulga, Phys. Rev. B **100**, 075415 (2019).
[51] C.-H. Hsu, P. Stano, J. Klinovaja, and D. Loss, Phys. Rev. Lett. **121**, 196801 (2018).
[52] K. Kudo, T. Yoshida, and Y. Hatsugai,arXiv:1905.03484.
[53] Z. Yan, arXiv:1905.11411.
[54] R.-X. Zhang, W. S. Cole, and S. Das Sarma, Phys. Rev. Lett. **122**, 187001 (2019).
[55] B. A. Bernevig, T. L. Hughes, and S.-C. Zhang, Science **314**, 1757 (2006).
[56] See Supplemental Material at http://link.aps.org/supplemental/10.1103/PhysRevLett.123.167001 for the full Hamiltonian $H_{\mathrm{FTS}}$, a derivation of topological conditions, definition of topological charge for nodal points, an analysis on the chiral symmetry protection of the Majorana flat bands, an estimate of interlayer exchange coupling from first-principles calculations, and a detailed analysis of potential and magnetic disorder effects.
[57] R. S. K. Mong, A. M. Essin, and J. E. Moore, Phys. Rev. B **81**, 245209 (2010).
[58] C.-X. Liu, arXiv:1304.6455.
[59] R.-X. Zhang and C.-X. Liu, Phys. Rev. B **91**, 115317 (2015).
[60] L. Fu and C. L. Kane, Phys. Rev. B **79**, 161408(R) (2009).
[61] J. Alicea, Rep. Prog. Phys. **75**, 076501 (2012).
[62] A. P. Schnyder and S. Ryu, Phys. Rev. B **84**, 060504(R) (2011).
[63] J. Yu and C.-X. Liu, Phys. Rev. B **98**, 104514 (2018).
[64] Y. Sun, W. Zhang, Y. Xing, F. Li, Y. Zhao, Z. Xia, L. Wang, X. Ma, Q.-K. Xue, and J. Wang, Sci. Rep. **4**, 6040 (2014).
[65] F. Nabeshima, Y. Imai, A. Ichinose, I. Tsukada, and A. Maeda, Jpn J. Appl. Phys. **56**, 020308 (2017).
[66] Y. Zhang, J. J. Lee, R. G. Moore, W. Li, M. Yi, M. Hashimoto, D. H. Lu, T. P. Devereaux, D.-H. Lee, and Z.-X. Shen, Phys. Rev. Lett. **117**, 117001 (2016).
[67] X. Wu, X. Liu, R. Thomale, and C.-X. Liu, arXiv:1905.10648.